Research Article | Vol. 11, No. 4 / 1 April 2020 / Biomedical Optics Express 1919
Biomedical Optics EXPRESS

Optical diffraction tomography with finite object support for the minimization of missing cone artifacts

WOJCIECH KRAUZE*

Warsaw University of Technology, Institute of Micromechanics and Photonics, Św. A. Boboli 8 Street, 02-525 Warsaw, Poland
*wojciech.krauze@pw.edu.pl

Abstract: Limited-angle optical diffraction tomography suffers from strong artifacts in tomographic reconstructions. Numerous algorithms, mainly based on regularization methods, have been developed recently to overcome this limitation. However, the quality of results still needs further improvement. Here I present a simple yet extremely effective method of increasing the reconstruction quality in limited angle optical diffraction tomography that can be combined with known tomographic algorithms. In the method a finite object support is generated from the object data and utilized in the reconstruction procedure as an additional strong regularizer. Practical aspects of this method are given together with examples of application.

1. Introduction

Limited-angle optical diffraction tomography (LAT) is an effective tool for the retrieval of the three-dimensional (3D) refractive index (RI) distribution of biological samples [1–3]. In this configuration a detector and a sample are stationary and the incidence angle of a laser illumination beam is altered. This guarantees fast and reliable investigation of biological samples that remain unperturbed in Petri dishes and glass slides during the whole measurement process. However, LAT suffers from strong artifacts in tomographic reconstructions calculated with standard algorithms, especially in the direction of the optical axis of the tomographic system [4]. Thus, multiple advanced reconstruction schemes have been developed in recent years to overcome this limitation, like edge-preserving regularization [5], total variation regularization [6], Gerchberg-Papoulis algorithm [7,8] or learning approach [9]. Another technique that has already been applied to x-ray computed tomography and magnetic resonance imaging [10–12] is utilization of finite object support in the reconstruction procedure. This finite object support can either be known *a priori* or be calculated with an auxiliary algorithm. It has been shown that supporting tomographic reconstruction algorithms with the information about investigated sample's extent reduces numerous artifacts in the final result. In LAT utilization of such support mainly addressees the "missing cone" artifacts that are always present due to limited angular range of acquired projections [8].

Utilization of finite object support in LAT is advantageous in practically all measurement cases at which biological cells are investigated. One of the most often measured samples are single biological cells and cell cultures with low confluency, where for each cell a separate support can be generated thus enhancing the reconstruction quality. However, even when specimens that cover the whole field of view are analyzed, like cell cultures with 100% confluency, a single support can be calculated. This support will not separate individual cells but, instead, will limit the specimen volume in the axial direction. This case is equally advantageous since in LAT the reconstruction artifacts are present mainly in the axial direction.

Despite the fact that utilization of finite object support in the reconstruction procedures has been proven to significantly increase quality of results, this method is very rarely used in optical

#386507 https://doi.org/10.1364/BOE.386507
Journal © 2020 Received 23 Dec 2019; revised 3 Feb 2020; accepted 3 Feb 2020; published 11 Mar 2020

Biomedical Optics EXPRESS

diffraction tomography. This may be due to the fact that in LAT it is very uncommon to know the object support *a priori* and the methods for automatic generation of this support are not known. The purpose of this paper is thus to promote and to show practical aspects of utilizing this simple yet extremely effective method of increasing the reconstruction quality in LAT, and in this sense it is a continuation and extension of the first description of this method [13].

2. Methods

In this Section, a description of the procedure for generation and utilization of object support in the reconstruction scheme is presented. First, a method for retrieval of investigated sample's artifact-free boundaries is shown. For this purpose an auxiliary regularized tomographic reconstruction is calculated. Later, examples of segmentation techniques that allow to transform such reconstruction into object support are given. Finally, a procedure for the utilization of a generated object support in the reconstruction algorithm is described.

The first step in generation of finite object support is the calculation of regularized tomographic reconstruction that will allow retrieving a reconstruction with correctly restored external geometry. During this step there is no focus on proper distribution of internal RI as it will be discarded after this step is calculated. Two examples of regularizers that can achieve such effect are total variation (TV) [13] and Haar wavelets [14]. In this paper utilization of TV will be shown as it is a popular regularizer which is implemented in freely available numerical libraries like TVReg [15,16] (Apache license 2.0, Matlab library), ASTRA Toolbox [17,18] (GPLv3 license, Matlab and Python library) or TIGRE [19,20] (BSD-3 license, Matlab and Python library).

In general, to calculate a TV-regularized reconstruction one needs to solve the following problem [6]:

$$\underset{f}{\text{minimize}} ||sA\vec{f} - s\vec{b}||_1 + \alpha||\nabla\vec{f}||_1 \tag{1}$$

where A is the system matrix, $\vec{f}$ is the reconstruction, $\vec{b}$ is the sinogram, ∇ is the gradient operator, α is a weighting factor which controls the "intensity" of the TV regularization and s is a scaling factor which helps to control the iteration step size. This minimization is carried out in an iterative manner and results in a tomographic reconstruction with correctly retrieved external geometry. As it was mentioned, the RI distribution of internal structures is erroneous. This is due to enforced piecewise constancy and the fact that Eq. (1) does not take light diffraction into account.

The result of the aforementioned operation is tomographic reconstruction with erroneous RI distribution, however with precisely retrieved external boundaries of the sample. In order to convert this information into finite object support, thresholding is carried out. The main difference between technical and biological objects in terms of thresholding is that bio-samples often have low-contrast parts that can extend beyond the main cellular body (e.g. pseudopods). Locally, the RI in such structures can have similar values to parts of the background, especially in the presence of reconstruction artifacts that are due to system aberrations. Conducting image segmentation for technical samples like optical fibers or microlenses is easier and can be carried out with multiple techniques, Otsu's method [21] among the most popular ones. For biological cells more advanced approaches are required. Two efficient tools are random walker [22] and watershed [23] algorithms. These procedures can operate on 3D matrices and are available in Matlab and Python. Both techniques require specifying markers which hold information about parts of the reconstruction that can be assigned to object and background classes, leaving the rest of the matrix as unknown that will be assigned to one of the above classes by the algorithm.

When the finite object support is generated by applying segmentation to the TV-regularized reconstruction, it can be utilized in the tomographic reconstruction procedure which takes light diffraction into account. For this purpose an iterative reconstruction algorithm is necessary - the support will be applied in each iteration in the signal domain. One example of such methods

Biomedical Optics EXPRESS

is Gerchberg-Papoulis (GP) method [7,8] in which Fourier transform of the reconstruction and inverse Fourier transform of the spectrum is calculated iteratively and in each domain constraints are applied. In the standard version of GP approach two constraints are utilized: nonnegativity in the signal domain and replenishment of known data in the spectrum domain. This approach allows for significant minimization of LAT artifacts in the calculated result. However, by adding finite object support as an additional constraint in the signal domain even further quality enhancement can be obtained, as is shown in the next Section.

3. Results

In order to shown the effectiveness of the object-support-assisted tomographic reconstruction, the method is applied to measurements of four representative samples: a cell from a HaCaT cell line, a physical cell phantom printed with a 3D nanoprinting device (Nanoscribe GmbH), described in [24], an epithelial cell and red blood cells. All samples were measured with a tomography setup based on an off-axis Mach-Zehnder interferometer working in a limited angle mode. The detailed description of the setup can be found in [25]. The sinograms consisted of 180 projections for the HaCaT cell and the 3d-printed cell phantom and of 90 projections for the remaining samples.

3.1. Total variation minimization

A set of TV-regularized tomographic reconstructions calculated with ASTRA Toolbox is shown in Fig. 1(a-b,e-f,i-j,m-n). The parameters from Eq. (1) were chosen experimentally as: $s = 0.2$, $\alpha = 0.002$. The process of finding these values included calculation of object supports for multiple values of s and α and assessing the results qualitatively. Since these values depend on the tomographic system parameters (e.g. number of projections, size of projections), it might be necessary to repeat this procedure for a different tomographic system. For comparison, on subfigures (c-d,g-h,k-l,o-p), the same cross-sections are shown for reconstructions calculated with the most basic tomographic reconstruction approach - unregularized Direct Inversion method [26] (also known as Fourier Diffraction Theorem algorithm or Wolf transform [9]). These last results show multiple artifacts caused by limited angular range of acquired projections, including elongation of the reconstruction in the optical axis direction (z-axis) and underestimation of the RI values, which is a common problem in LAT [4,27]. When analyzing the Fig. 1 it is clear that TV regularization retrieves true external geometry of analyzed samples. What is more, average RI distribution is no longer underestimated. However, as it will be shown later in the paper, the lateral and axial resolution of these reconstructions is limited. These conclusions are true for biological cells with a simple structure (like the HaCaT cell and cell phantom) but also for biological cells with a complex structure (the epithelial cell) and for multiple cells in the field-of-view (the set of red blood cells). Note that the red contour visible in the Figure will be explained in the next subsection.

3.2. Thresholding

The reconstructions shown in Fig. 1(a-b,e-f,i-j,m-n) underwent the segmentation procedure with the watershed algorithm and boundaries of the resulting mask are superimposed on all cross-sections in the Figure. The superimposition of the mask with subfigures (a-b,e-f,i-j,m-n) shows the high precision of the segmentation process, whereas the superimposition with subfigures (c-d,g-h,k-l,o-p) shows how the retrieved geometry looks when compared to the Direct Inversion reconstruction. To quantitatively assess the precision of the support-generation process, the volume of the object support generated for the cell phantom (Fig. 1(e-h)) was compared with the true volume of the phantom, which equals $3826 \mu m^3$. The calculation was carried out simply by counting all nonzero voxels in the generated support and multiplying this number by the volume of a single voxel. The calculated volume equals $3788 \mu m^3$, which means that the relative error of the volume equals 1%.

Biomedical Optics EXPRESS

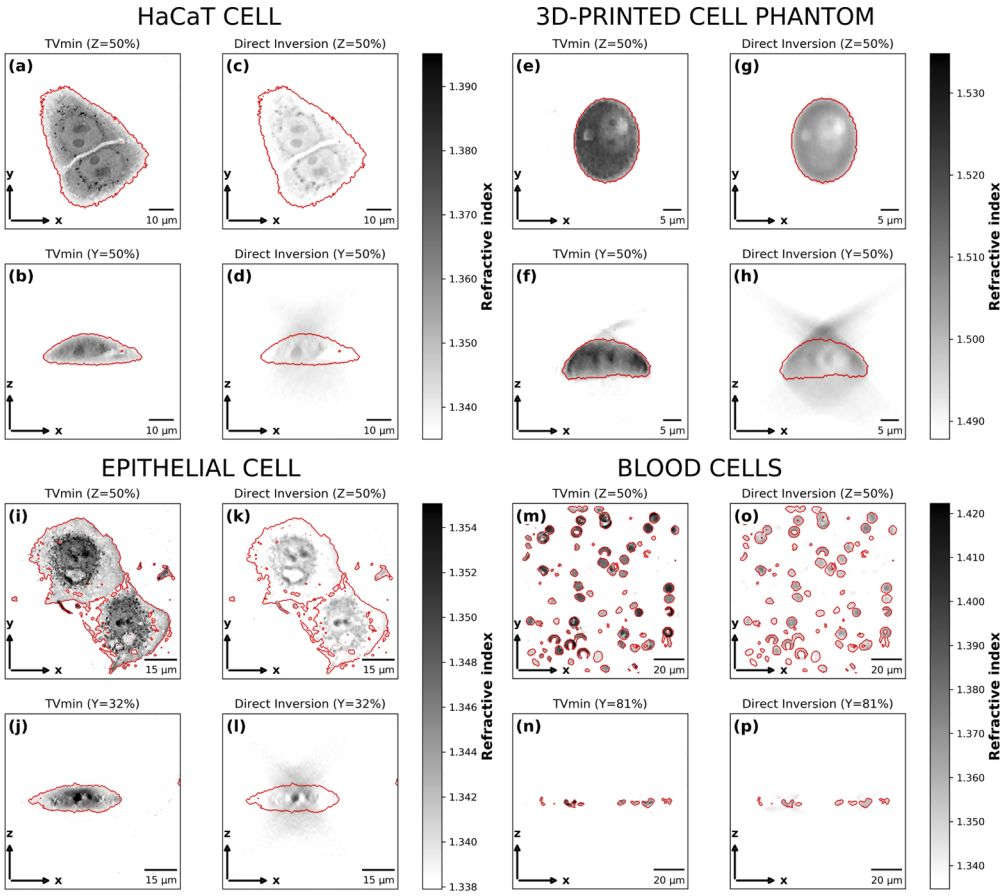

Fig. 1. Effectiveness of the TV regularization and segmentation in finite object support generation. Figure presents 4 tomographic reconstructions: (a-d) of a HaCaT cell, (e-h) of a 3d-printed cell phantom, (i-l) of an epithelial cell and (m-p) of blood cells. Each dataset shows x-y and x-z cross-sections through the tomographic reconstruction calculated with total variation regularization (TVmin) and cross-sections through the reconstruction calculated with the Direct Inversion method. The support constraint calculated by applying segmentation to TVmin reconstruction is shown as red contour superimposed on all cross-sections.

3.3. Integration of the object support with the reconstruction procedure

In order to present an example of a practical implementation of the object support, its combination with GP algorithm has been carried out. In Fig. 2 two datasets are presented: of the HaCaT cell and of the cell phantom. In the Figure, the comparison of a classic GP approach with GP approach assisted with object support (GP-SC) is presented. Additionally, GP-SC reconstructions are calculated in two ways: one by applying binarized object support (GP-SC-BINARY) and one with the binarized object support that additionally underwent gaussian filtering to smoothen the edges of the support (GP-SC-SMOOTH). The purpose of the second approach is to minimize the small errors that can potentially be present at the mask boundaries. Figure 2 clearly shows a significant reconstruction quality increase when the object support is utilized. The object boundaries are correctly retrieved (both test objects should have flat bottom boundary), there is no elongation of the results in the direction of the optical axis (Z-axis) and the average RI is corrected. When comparing binary and smooth object supports, one can notice that the latter

Biomedical Optics EXPRESS

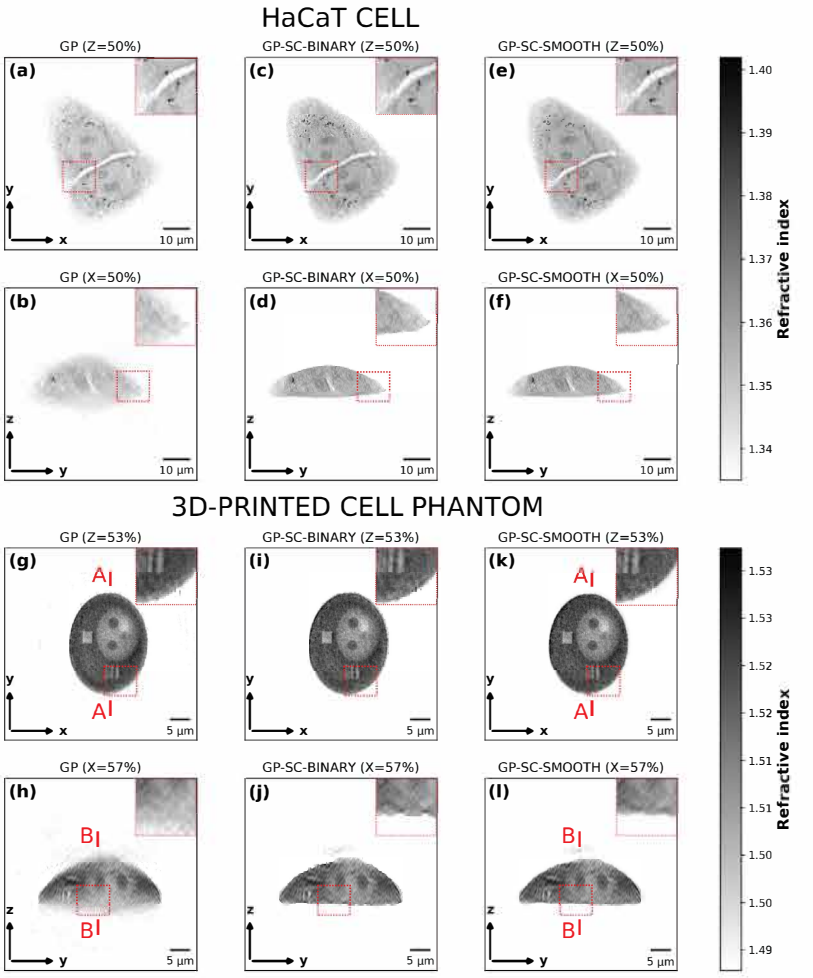

Fig. 2. Comparison of GP reconstructions (a-b,g-h) with GP-SC reconstructions that utilize object support constraint in the form of (c-d,i-j) binary mask and (e-f,k-l) mask with smooth edges. Area marked with the red rectangle is shown magnified.

approach results in minimized errors at the boundaries - this is especially visible in the cell phantom when comparing magnified regions in subfigures (j) and (l). The corrected distribution of RI is also shown in Fig. 3, where comparison of GP and GP-SC-SMOOTH reconstructions with numerical model of the cell phantom is carried out. It can be noticed that when support constraint is utilized not only the boundaries of the specimen are better retrieved but also that RI values near object boundaries are closer to the ground truth. What is also interesting, by utilizing object support in the tomographic reconstruction procedure, the total reconstruction time decreases. Calculation of the reconstruction shown in Fig. 2(g-h) took 21 minutes whereas the calculation of the result shown in Fig. 2(i-j) and (k-l) took 9 minutes (this includes the time required to calculate the TV-regularized reconstruction from which the support is generated). The reasons for this time decrease is associated with the fact that GP algorithm requires significantly fewer iterations to converge to the solution when object support is used.

Biomedical Optics EXPRESS

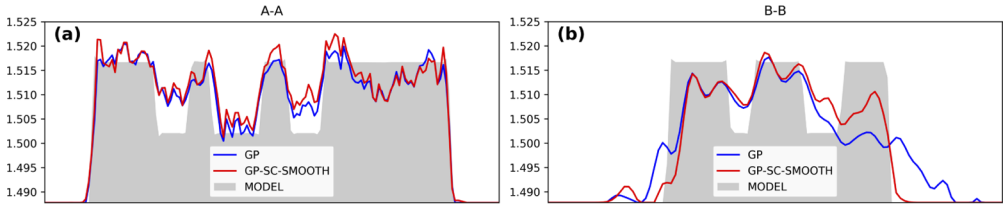

Fig. 3. Cross-sections showing a comparison of GP and GP-SC-SMOOTH reconstructions with the numerical model of the cell phantom: (a) y-cross-sections along A-A line marked in Fig. 2 and (b) z-cross-sections along B-B line marked in Fig. 2.

Figure 2 presents the final result obtained with the use of the object support. However, it is interesting to analyze how this result compares to pure TV-regularized reconstruction that was presented in Fig. 1. This comparison is shown in Fig. 4, and the presented samples are the HaCaT cell and the 3d-printed cell phantom. This allows to assess what is the effect of taking light diffraction into account during the reconstruction procedure on the quality of results. It also explains why it is advantageous to create an object support out of a TV-regularized reconstruction and pass it to diffraction-based algorithm instead of leaving the TV-regularized reconstruction as the final result. When analyzing the Fig. 4, it is clear that the TV-regularized reconstruction retrieves external geometry with high precision, however the resolution of internal structures

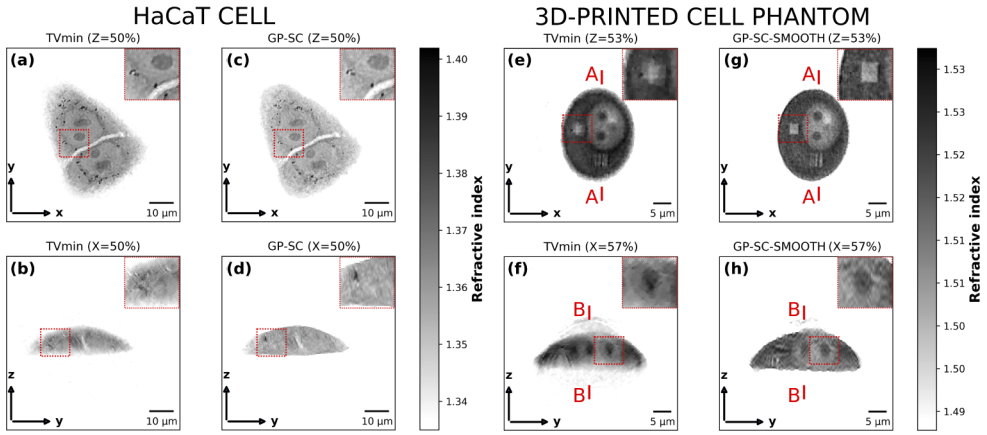

Fig. 4. Comparison of a reconstruction calculated with TV-regularization (TVmin) which does not take light diffraction into account with a reconstruction calculated with diffraction-based GP-SC-SMOOTH algorithm which utilizes support constraint. Area marked with the red rectangle is shown magnified.

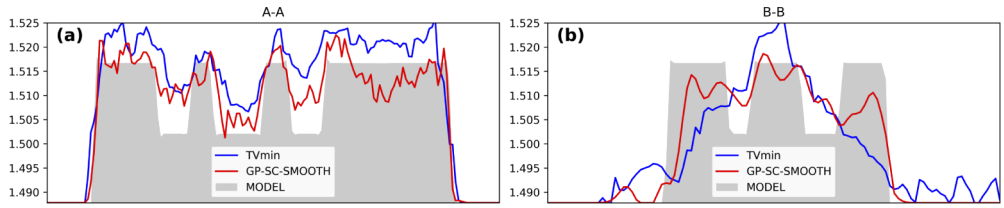

Fig. 5. Cross-sections showing a comparison of TVmin and GP-SC-SMOOTH reconstructions with the numerical model of the cell phantom: (a) y-cross-sections along A-A line marked in Fig. 4 and (b) z-cross-sections along B-B line marked in Fig. 4.

Biomedical Optics EXPRESS

is significantly higher when GP-SC method is used, which is an expected results since GP-SC approach takes light diffraction into account. This is especially visible in the magnified regions. Further comparison is shown in Fig. 5 where cross-sections along lines marked in Fig. 4 are presented and compared with RI distribution of the numerical model of the cell phantom. It is clear that the TV-regularized result has not only decreased resolution when compared to GP-SC reconstruction, but also that its average RI is overestimated. This is corrected when diffraction-based method is used.

4. Conclusions

In the paper it has been shown that by applying a relatively simple method of generating a smooth-edged finite object support one can significantly increase the quality of tomographic reconstructions by minimizing LAT artifacts that are due to the "missing cone" problem. Practical aspects of this approach have been given, including values of the parameters for the support generation, segmentation methods and an example of integration of the support constraint with a reconstruction algorithm. This method can be utilized when analyzing single biological cells, multiple biological cells or technical samples and can be successfully applied to virtually all iterative reconstruction algorithms. In practice, the proposed approach should be applied to all tomographic measurements cases where high quality 3D RI distribution is crucial. If, however, the purpose of the measurement is to retrieve the central $x - y$ cross-section of the reconstruction, which is a commonly found mode of operation, the proposed method will not provide significant advantage.

Funding

Fundacja na rzecz Nauki Polskiej (TEAM TECH/2016-1/4, START).

Acknowledgments

The research leading to the described results was carried out within the program TEAM TECH/2016-1/4 of Foundation for Polish Science, co-financed by the European Union under the European Regional Development Fund. I would also like to acknowledge the START scholarship of Foundation for Polish Science and the support from the statutory funds of Warsaw University of Technology, Mechatronics Department.

Disclosures

The authors declare that there are no conflicts of interest related to this article.

References

1. O. Haeberlé, K. Belkebir, H. Giovaninni, and A. Sentenac, "Tomographic diffractive microscopy: basics, techniques and perspectives," J. Mod. Opt. **57**(9), 686–699 (2010).
2. D. Jin, R. Zhou, Z. Yaqoob, and P. T. C. So, "Tomographic phase microscopy : Principles and applications in bioimaging," J. Opt. Soc. Am. B **34**(5), B64–B77 (2017).
3. A. Kuś, W. Krauze, P. L. Makowski, and M. Kujawińska, "Holographic tomography: hardware and software solutions for 3D quantitative biomedical imaging (Invited paper)," ETRI Journal **41**(1), 61–72 (2019).
4. M. Kujawińska, W. Krauze, M. Baczewska, A. Kuś, and M. Ziemczonok, "Comparative study of laboratory and commercial limited-angle holographic tomography setups," Proc. SPIE **10887**, 1088708 (2019).
5. P. Charbonnier, L. Blanc-Féraud, G. Aubert, and M. Barlaud, "Deterministic edge-preserving regularization in computed imaging," IEEE Trans. on Image Process. **6**(2), 298–311 (1997).
6. E. Y. Sidky, C.-M. Kao, and X. Pan, "Accurate image reconstruction from few-views and limited-angle data in divergent-beam CT," J. X-Ray Sci. Technol. **14**, 119–139 (2006).
7. A. Papoulis, "A new algorithm in spectral analysis and band-limited extrapolation," IEEE Trans. Circuits Syst. **22**(9), 735–742 (1975).
8. J. Lim, K. Lee, K. H. Jin, S. Shin, S. Lee, Y. Park, and J. C. Ye, "Comparative study of iterative reconstruction algorithms for missing cone problems in optical diffraction tomography," Opt. Express **23**(13), 16933–16948 (2015).

Biomedical Optics EXPRESS

9. J. Lim, A. B. Ayoub, E. E. Antoine, and D. Psaltis, "High-fidelity optical diffraction tomography of multiple scattering samples," Light: Sci. Appl. **8**(1), 82 (2019).
10. P.-C. Lee, "Multigrid iterative method with adaptive spatial support for computed tomography reconstruction from few-view data," Proc. SPIE **9033**, 90333C (2014).
11. A. Dogandžić, R. Gu, and K. Qiu, "Mask iterative hard thresholding algorithms for sparse image reconstruction of objects with known contour," in *2011 Conference Record of the Forty Fifth Asilomar Conference on Signals, Systems and Computers (ASILOMAR)*, (2011), 2111–2116.
12. A. Manduca, J. D. Trzasko, and Z. Li, "Compressive sensing of images with a priori known spatial support," Proc. SPIE **7622**, 762223 (2010).
13. W. Krauze, P. Makowski, M. Kujawińska, and A. Kuś, "Generalized total variation iterative constraint strategy in limited angle optical diffraction tomography," Opt. Express **24**(5), 4924–4936 (2016).
14. P. L. Makowski, "Redundant haar wavelet regularization in sparse-view optical diffraction tomography of microbiological structures," Proc. SPIE **10834**, 108341U (2018).
15. T. L. Jensen, J. H. Jørgensen, P. C. Hansen, and S. H. Jensen, "Implementation of an optimal first-order method for strongly convex total variation regularization," Bit. Numer. Math. **52**(2), 329–356 (2012).
16. "Tvreg," https://github.com/jakobsj/TVReg. Accessed: 2019-10-15.
17. W. van Aarle, W. J. Palenstijn, J. Cant, E. Janssens, F. Bleichrodt, A. Dabravolski, J. De Beenhouwer, K. J. Batenburg, and J. Sijbers, "Fast and flexible x-ray tomography using the astra toolbox," Opt. Express **24**(22), 25129–25147 (2016).
18. "Astra toolbox," https://github.com/astra-toolbox/astra-toolbox. Accessed: 2019-10-15.
19. A. Biguri, M. Dosanjh, S. Hancock, and M. Soleimani, "Tigre: a matlab-gpu toolbox for CBCT image reconstruction," Biomed. Phys. Eng. Express **2**(5), 055010 (2016).
20. "Tigre," https://github.com/CERN/TIGRE. Accessed: 2019-10-15.
21. N. Otsu, "A threshold selection method from gray-level histograms," IEEE Trans. Syst., Man, Cybern. **9**(1), 62–66 (1979).
22. L. Grady, "Random walks for image segmentation," IEEE Trans. Pattern Anal. Mach. Intell. **28**(11), 1768–1783 (2006).
23. P. J. Soille and M. M. Ansoult, "Automated basin delineation from digital elevation models using mathematical morphology," Signal Processing **20**(2), 171–182 (1990).
24. M. Ziemczonok, A. Kuś, P. Wasylczyk, and M. Kujawińska, "3d-printed biological cell phantom for testing 3D quantitative phase imaging systems," Sci. Rep. **9**(1), 18872 (2019).
25. A. Kuś, "Illumination-related errors in limited-angle optical diffraction tomography," Appl. Opt. **56**(33), 9247–9256 (2017).
26. E. Wolf, "Three-dimensional structure determination of semi-transparent objects from holographic data," Opt. Commun. **1**(4), 153–156 (1969).
27. Y. Sung and R. R. Dasari, "Deterministic regularization of three-dimensional optical diffraction tomography," J. Opt. Soc. Am. A **28**(8), 1554–1561 (2011).